QUANTUM TRANSFORMATION : THE ANALYSIS OF QUANTUM RECTIFIER-INVERTERS

C. T. Rim and G. H. Cho

Dept. of Electrical Engineering, Korea Advanced Institute of Science and Technology

P.O.Box 150 Chongryang, Seoul 130-650, Korea (Tel. 966-1931 ext. 3723)

ABSTRACT

The quantum rectifier-inverters becoming a new class of cyclo-converters are analyzed by a new analysis based on *quantum transformation*. The procedure of the transformation is explained and then it is applied to the quantum converters to obtain equivalent conventional circuits. Then it is analyzed by the circuit D-Q transformation, from which the DC voltage gain is derived. Finally the gain is verified by the time-domain simulations with good agreements. The switching patterns, or equivalently the control laws, of the quantum converters are determined by a very simple logic circuit composed of only two EXOR gates when those of the equivalent rectifier-inverters are already known. From this paper it is found that the operation of the quantum converters is tightly related with that of the conventional converters via the proposed quantum transformation.

I. INTRODUCTION

Recent years a new class of the quantum converters which are found to be a kind of resonant converters are suggested [1-3]. Since their switching frequency and phase are fixed to resonant frequency and zero degrees, respectively, the controls of them are performed by the time domain selection of discrete pulses. The name *quantum* stems from the quantized output level and quantized time domain control. Since they operate at either current or voltage zero switching points, their switching loss and stress are negligible, which is crucial feature necessary for high frequency application.

It has been verified that the quantum DC/DC converters are equivalent to the conventional PWM DC/DC converters [2]. It is natural to expect the equivalent conventional converters for the quantum rectifier-inverters also.

In this paper an easy way to analyze the quantum converters, *quantum transformation* is proposed, such that the complex unfamiliar quantum converters can be regarded as the simple and familiar conventional converters. And the method to determine the switching patterns for the control of the quantum converters are suggested. Finally the recently proposed circuit D-Q transformation [4] is used to analyze the equivalent converters with ease.

II QUANTUM TRANSFORMATION

The systems to be modeled are shown in Fig. 1 and Fig. 2 which are named as *Quantum Parallel-link Rectifier-Inverter* (QPRI) and *Quantum Series-link Rectifier- Inverter* (QSRI), respectively. It is assumed that all circuit elements are linear, switches are ideal bidirectional, and switching harmonics are negligible.

A. Preliminaries

Consider first the resonant circuit shown in Fig. 3. The transfer function of Fig. 3 (a) is

$$G_1(s)=\frac{I_L(s)}{V_S(s)}=\frac{1}{sL+\frac{1}{sC}} \quad . \tag{1}$$

(1) can be used to determine the i_L from the given v_s as shown in Fig.4. However this is improper to determine the envelope of i_L, which is practically meaningful. What we want to know is the average value of modulated i_L for given modulated v_s as shown in Fig.4.

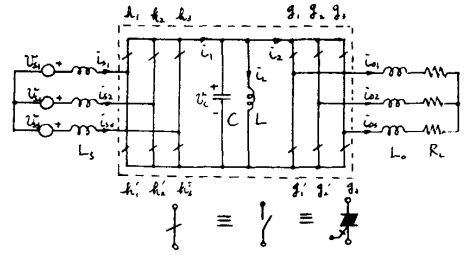

Fig. 1 Quantum parallel link rectifier-inverter.

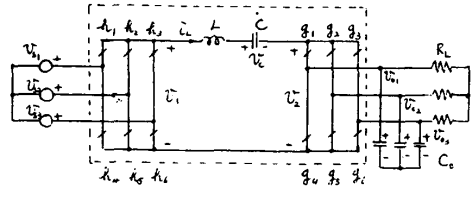

Fig. 2 Quantum series link rectifier-inverter.

The frequency of source voltage is set to the resonant frequency,

$$f_s=\frac{1}{T}=\frac{\omega}{2\pi}=\frac{1}{2\pi(LC)^{\frac{1}{2}}} \tag{2}$$

Then during the period A of Fig. 4(b) the energy of resonant tank increases, during B that is kept constant, and during C that decreases. The inductor current is computed as follows [1] :

$$i_L=[I_p(k-1)+2S(\frac{C}{L})^{\frac{1}{2}}V_s]\cdot q(t)\cdot\sin\omega(t-\frac{kT}{2})$$
$$\text{for } \frac{kT}{2}<t<\frac{k+1}{2}T \quad , S=1 \text{ for } A,$$
$$S=0 \text{ for } B,\ S=-1 \text{ for } C \tag{3}$$

where

$$I_p(k)=\text{ peak of } [i_L\cdot q(t)]$$
$$q(t)=-1+2u(t)-2u(t-\frac{T}{2})+\cdots \tag{4}$$

$u(t)$ is unit step function. Now the quantum transformation is defined for arbitrary variable $x(t)$ as

$$x^*(t)\equiv q(t)\cdot\overline{x(t)}=q(t)\frac{2}{T}\int_{kT/2}^{(k+1)2T}x(t)\,dt$$
$$\text{for } \frac{kT}{2}<t<\frac{k+1}{2}T \quad . \tag{5}$$

89CH2792-0/89/0000-1081$01.00 © 1989 IEEE

(a) original circuit. (b) equivalent circuit.

Fig. 3 Equivalent series resonant tank.

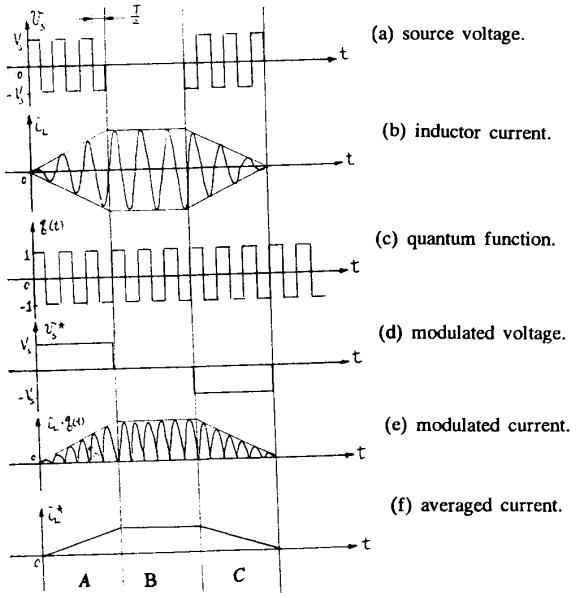

Fig. 4 Waveforms of Fig. 3.

Then the quantum transformed voltage and inductor current become

$$v_s^* \equiv q(t)\overline{v_s} = q(t)v_s = q(t)[V_s q(t)S] = [q(t)]^2 V_s S = V_s S \qquad (6a)$$

$$i_L^* \equiv q(t)\overline{i_L} = q(t)[I_p(k-1) + 2S(\frac{C}{L})^{\frac{1}{2}} V_s] q(t)\frac{2}{\pi}$$

$$= [I_p(k-1) + 2S(\frac{C}{L})^{\frac{1}{2}} V_s]\frac{2}{\pi} \qquad (6b)$$

where

$$[q(t)]^2 = 1 \quad . \qquad (7)$$

From (3) and (4) it is found that

$$i_L = I_p(k)\frac{2}{\pi}q(t) \quad . \qquad (8)$$

Applying (8) to (6b) results in

$$i_L^*\Big|_{t=\frac{kT}{2}} = \frac{2}{\pi}I_p(k) = \frac{2}{\pi}I_p(k-1) + \frac{4}{\pi}S(\frac{C}{L})^{\frac{1}{2}} V_s$$

$$= i_L^*\Big|_{t=\frac{(k-1)}{2}T} + \frac{4}{\pi}S(\frac{C}{L})^{\frac{1}{2}} V_s \quad . \qquad (9)$$

Then the derivative of the current is

$$i_L^* = \frac{i_L^*\Big|_{t=\frac{kT}{2}} - i_L^*\Big|_{t=\frac{(k-1)}{2}T}}{T/2} = \frac{2}{T}\frac{4}{\pi}S(\frac{C}{L})^{\frac{1}{2}} V_s$$

$$= (\frac{2}{\pi})^2 \frac{SV_s}{L} = \frac{V_s^*}{L^*} \qquad (10)$$

where

$$L^* = (\frac{\pi}{2})^2 L \approx 2.5L \quad . \qquad (11)$$

The circuit reconstruction of (10) is Fig. 3(b). The transfer function of it is

$$G_2(s) = \frac{I_L(s)^*}{V_S(s)^*} = \frac{1}{sL^*} \qquad (12)$$

Comparing (12) with (1), it can be seen that the transfer function is changed in large scale by the quantum transformation.

By similar manipulation the parallel resonant circuit becomes a capacitor by the quantum transformation as shown in Fig. 5. The equivalent capacitor is

$$C^* = (\frac{\pi}{2})^2 C \quad . \qquad (13)$$

B. Quantum Transformation of QPRI.

Using the results of the preliminary the circuit shown in Fig. 1 is transformed to an equivalent circuit in this section.

The system equation is found to be

$$L_s \dot{i}_{sN} = v_{sN} - s_N(t)v_c$$
$$L_o \dot{i}_{oN} = w_N(t)v_c - i_{oN}R_L$$

$$i_1 = \sum_{N=1}^{3} s_N(t)i_{sN}$$

$$i_2 = \sum_{N=1}^{3} w_N(t)i_{oN} \quad , \quad \text{for } N = 1, 2, 3 \qquad (14)$$

where

$$s_N(t) = h_N - h_N'$$
$$w_N(t) = g_N - g_N' \quad , \quad \text{for } N = 1, 2, 3 \quad . \qquad (15)$$

Considering (7), (14) becomes

$$L_s \dot{i}_{sN} = v_{sN} - s_N(t)v_c[q(t)]^2$$
$$= v_{sN} - [s_N(t)q(t)]\cdot[q(t)v_c]$$
$$\approx v_{sN} - s_N^*(t)v_c^*$$
$$L_o \dot{i}_{oN} = [w_N(t)q(t)]\cdot[q(t)v_c] - i_{oN}R_L$$
$$\approx w_N^*(t)v_c^* - i_{oN}R_L$$

$$i_1^* \equiv q(t)\overline{i_1} = q(t)\sum_{N=1}^{3} s_N(t)i_{sN}$$
$$= \sum_{N=1}^{3} s_N^*(t)i_{sN}$$

$$i_2^* \equiv q(t)\overline{i_2} = \sum_{N=1}^{3} w_N^*(t)i_{oN} \quad , \quad \text{for } N = 1, 2, 3 \quad . \qquad (16)$$

The approximation is used when it is required to ignore the high frequency harmonics. Considering the result of Fig. 5 the circuit reconstruction of (16) is Fig. 6, which is the quantum transformed equivalent circuit of Fig. 1. The dotted lines of Fig. 1 and Fig. 6 indicate the portion where the quantum transformation is taken.

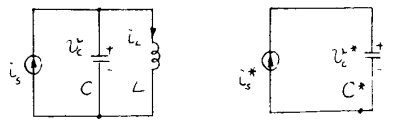

(a) original circuit. (b) equivalent circuit.

Fig. 5 Equivalent parallel resonant tank.

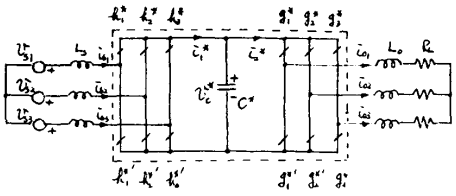

Fig. 6 Quantum transformed QPRI.

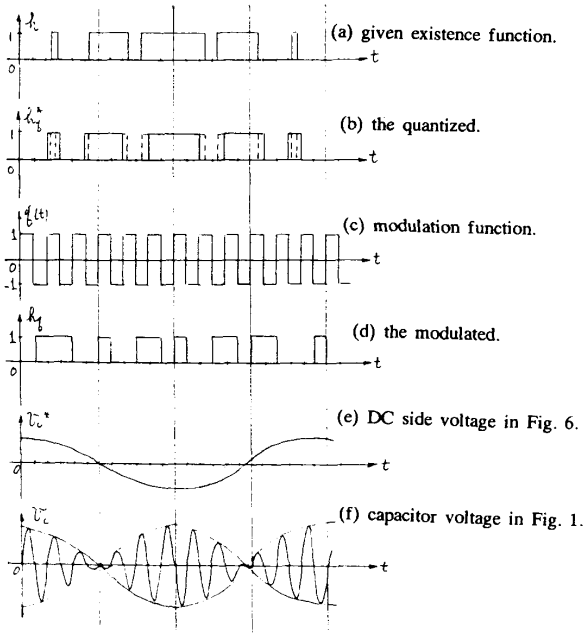

Fig. 7 The relationship between Fig. 1 and Fig. 6.

The existence functions are as follows:

$$s_N^*(t)=h_N^*-h_N^{*\prime}=q(t)s_N(t)=q(t)[h_N-h_N']$$

$$\dashrightarrow\quad h_N^*=\begin{cases}h_N & \text{for}\quad q(t)=1\\ h_N' & \text{for}\quad q(t)=-1\end{cases}\qquad(17a)$$

$$w_N^*(t)=g_N^*-g_N^{*\prime}=q(t)w_N(t)=q(t)[g_N-g_N']$$

$$\dashrightarrow\quad g_N^*=\begin{cases}g_N & \text{for}\quad q(t)=1\\ g_N' & \text{for}\quad q(t)=-1\end{cases}$$

$$\text{for}\quad N=1,\ 2,\ 3\qquad(17b)$$

(17) can be used to find the appropriate h_N for given h_N^* as shown in Fig. 7. If any wanted existence function h is given then it is truncated as shown in Fig. 7 (b). And it is modulated and then the quantum existence function, h_q is generated as follows:

$$h_q=\begin{cases}h_q^* & \text{for}\quad q(t)=1\\ h_q^{*\prime} & \text{for}\quad q(t)=-1\end{cases}\qquad(18)$$

If the DC side voltage of Fig. 6 is given as shown in Fig. 7(e) then the capacitor voltage can be predicted considering the quantum transformation as shown in Fig. 7(f).

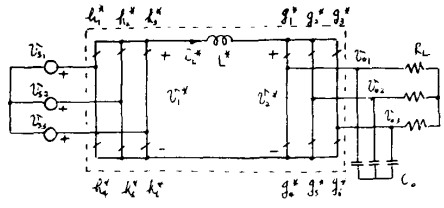

Fig. 8 Quantum transformed QSRI.

C. Quantum Transformation of QSRI

By similar procedure the QSRI as shown in Fig. 2 can be quantum transformed as shown in Fig. 8. The existence functions are, however, a little different.

Since it is found from Fig. 2 that

$$v_1=\sum_{N=1}^{3}(h_N-h_{N+3})v_{sN}=\sum_{N=1}^{3}s_N(t)v_{sN}\qquad(19a)$$

$$v_1^*=q(t)v_1=q(t)\sum_{N=1}^{3}s_N(t)v_{sN}=\sum_{N=1}^{3}s_N^*(t)v_{sN}\ ,\qquad(19b)$$

it can be seen that

$$s_N^*(t)=h_N^*-h_{N+3}^*=q(t)s_N(t)=q(t)[h_N-h_{N+3}]\qquad(20a)$$

$$\dashrightarrow\quad h_N^*=\begin{cases}h_N & \text{for}\quad q(t)=1\\ h_{N+3} & \text{for}\quad q(t)=-1\end{cases}$$

$$h_{N+3}^*=\begin{cases}h_{N+3} & \text{for}\quad q(t)=1\\ h_N & \text{for}\quad q(t)=-1\end{cases}\ .\qquad(20b)$$

What we want to do is to determine the switch pattern of Fig. 2 when that of Fig. 8 is given. This can be accomplished using (20)

D. Logic Gate For The Switch Pattern Generation.

When the switch pattern of conventional rectifier-inverter is given that of quantum rectifier-inverter can be generated by an appropriate logic gate.

Observing (17) and (20) it can be seen that the logic gate shown in Fig. 9 works as the appropriate pattern generator.

The inputs are as follows:

$$[h_a,h_b]=\begin{cases}[h_N,\ h_N'] & \text{for}\quad QPRI\\ [h_N,h_{N+3}] & \text{for}\quad QSRI\end{cases}$$

$$q_d=\begin{cases}1 & \text{for}\quad q(t)=1\\ 0 & \text{for}\quad q(t)=-1\end{cases}\qquad(21)$$

The logic gate has the property that input output switch patterns can be exchanged by the same gate; that is, if the input is $[h_a^*,h_b^*]$ then the output becomes $[h_a,h_b]$.

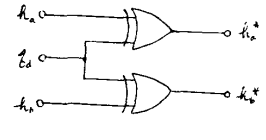

Fig. 9 Switching pattern generator.

III. CIRCUIT D-Q TRANSFORMATION

The conventional rectifier-inverters as shown in Fig. 6 and Fig. 8 can be easily analyzed by a new analysis technique, circuit D-Q transformation [4]. The equivalent circuits are drawn as shown in Fig. 10 and Fig. 11.

The AC transfer functions can be derived from Fig. 10 and Fig. 11. Those who are interested in the procedure of this, please see the reference [4].

In this paper only DC analysis is suggested though AC analysis is also possible. The DC circuits of Fig. 10 and Fig. 11 are Fig. 12 and Fig. 13, respectively.

$$V_d = I_3 R_L = \frac{I_2}{D_2} R_L = \frac{D_1}{D_2} I_1 R_L = \frac{D_1}{D_2} \frac{V_s \sin\phi}{\omega_1 L_s} R_L$$

$$V_q = \omega_2 L_o I_3 = \omega_2 L_o \frac{V_d}{R_L} \tag{22}$$

ϕ is the phase difference between the source voltage and input side fundamental switching function. From (22) it can be seen that the DC transfer function G_V becomes

$$G_V \equiv \frac{V_o}{V_s} = \frac{[V_d^2 + V_q^2]^{\frac{1}{2}}}{V_s}$$

$$= \frac{D_1}{D_2} \frac{\sin\phi}{\omega_1 L_s} R_L \cdot [1 + (\frac{\omega_2 L_o}{R_L})^2]^{\frac{1}{2}} . \tag{23}$$

By similar procedure the DC transfer function of Fig. 13 becomes

$$G_V = \frac{D_1}{D_2} \cos\phi [1 + (\omega C R_L)^2]^{\frac{1}{2}} \tag{24}$$

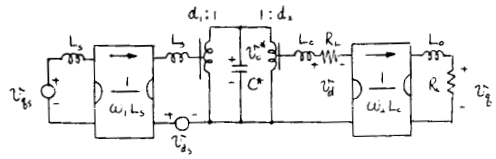

Fig. 10 Circuit D-Q transformation of Fig. 6.

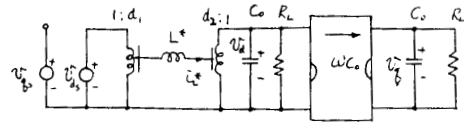

Fig. 11 Circuit D-Q transformation of Fig. 8.

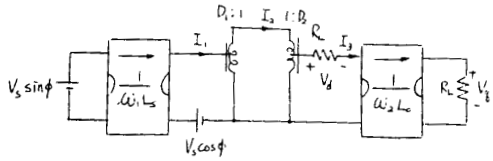

Fig. 12 DC circuit of Fig. 10.

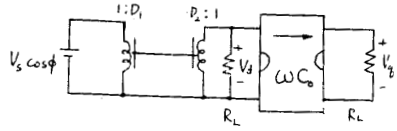

Fig. 13 DC circuit of Fig. 11.

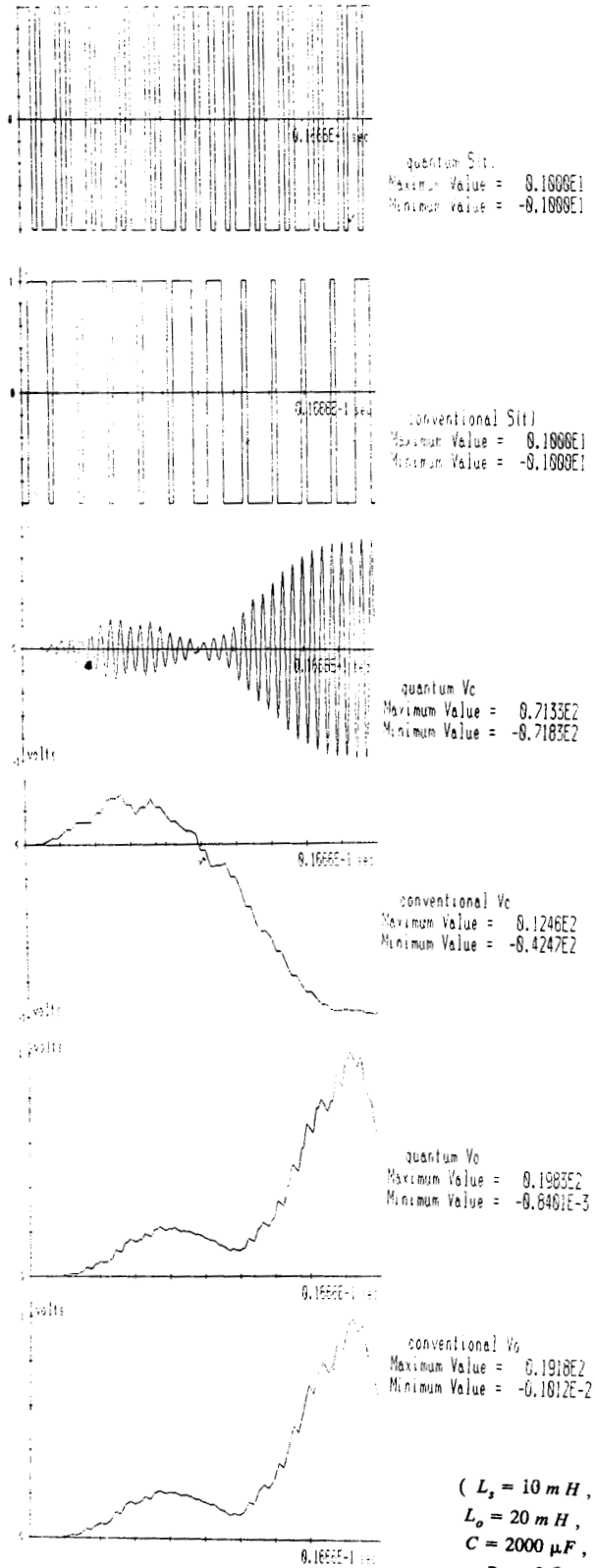

Fig. 14 Simulated waveforms of Fig. 1 and Fig. 6.

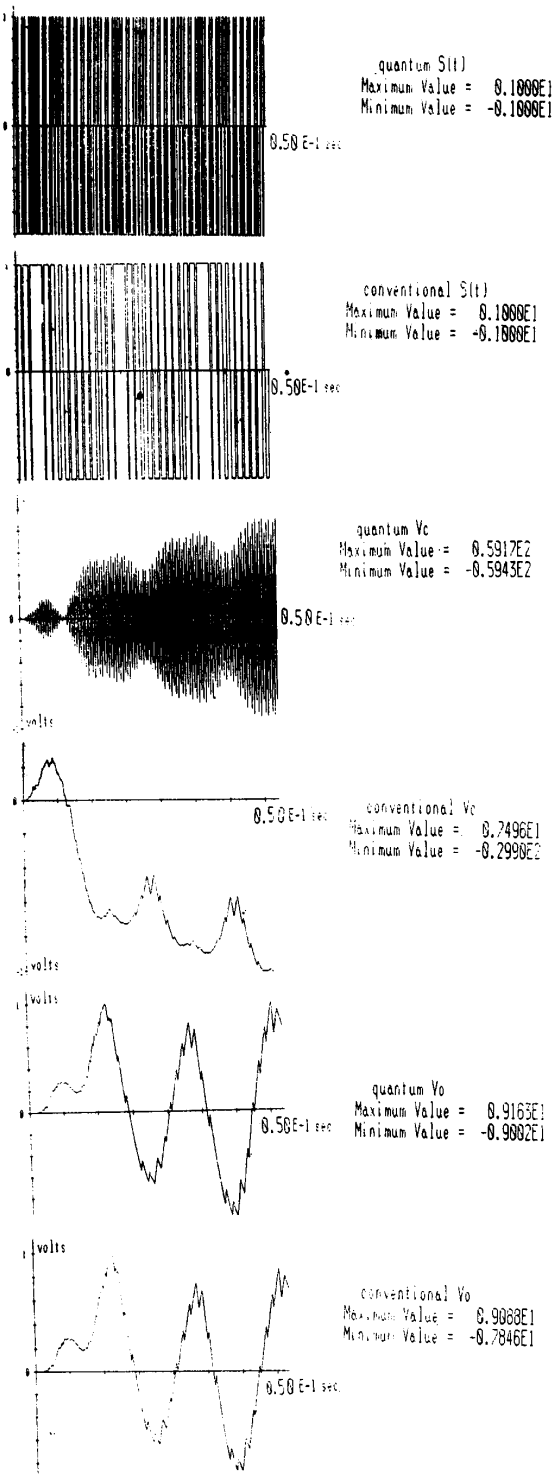

Fig. 15 Simulated waveforms of Fig. 1 and Fig. 6.

($L_s = 20\ mH$, $L_o = 10\ mH$, $C = 2000\ \mu F$, $R_L = 2\ \Omega$)

It can be seen from (23) and (24) the output voltage can be controlled by switch patterns: D_1, D_2 and ϕ. The dependencies of ϕ on QSRI and QPRI are, however, quite different. (23) and (24) can be used to determine the operating point when load conditions are given. The output voltage ranges from zero to its maximum. And it is certainly possible to vary the input power factor though this is not proved here.

IV. SIMULATION

To verify the quantum transformation the circuits of Fig. 1 and Fig. 6 are compared through simulation. The circuit parameters are selected practically as follows:

$$V_s = 100\ V, \quad \omega_1 = \omega_2 = 120\pi\ \text{rad/sec}$$

$$f_s = 2160\ Hz, \quad \phi = \frac{\pi}{6} \tag{25}$$

The switch pattern is let be just the same as Fig. 7 and it is assumed that three phases are balanced. The simulation is done by direct computation of (14), (16) and resonant circuit equations [1].

Figs. 14-15 show that how the operation of the quantum converter is connected with that of the corresponding conventional converter assuming zero initial conditions. As can be seen from the figures, the PWM patterns of the quantum converter are not easily recognizable, however they are merely the switching patterns of the conventional converter multiplied by the quantum function $q(t)$ as can be identified from the figures. And the output waveforms of the quantum converter are nearly the same as those of the conventional converter except only the very small portion of the high frequency harmonics.

It can be seen from the simulation that the quantum transformation is very useful for the envelope prediction and switch pattern generation of the quantum converters as well as the analysis of them.

V. CONCLUSION

A new concept, *quantum transformation*, by which the equivalent conventional circuits are derived from the QPRI and the QSRI is proposed in this paper. It is found that the role of a parallel (or series) resonant link in the quantum converter is just the same as that of a capacitor (or inductor) in the conventional converter by the transformation. The switch patterns of the quantum converters which are highly confusing in fact are now easily determined by a simple logic gate which is composed of only two EXOR gates when the switch patterns of the equivalent conventional converters are known.

Now the analyses of the quantum converters become merely those of conventional converters by the proposed transformation. The analysis based on the circuit D-Q transformation of the quantum transformed circuits also shows that the outputs of the quantum converters can be controlled from zero to their maximums by moderate switching patterns.

REFERENCES

[1] G. B. Joung, C. T. Rim and G. H. Cho," An integral cycle-mode control of series resonant converters," IEEE Power Electronics Specialists Conf. Rec., 1988, pp. 575-582.

[2] G. B. Joung, C. T. Rim and G. H. Cho," Modeling of quantum series resonant converters- Controlled by integral cycle mode," IEEE-IAS Conf. Rec., 1988, pp. 821-826.

[3] T. A. Lipo, " Recent progress in the development of solid-state AC motor drives," IEEE Trans. Power Electronics, Vol. PE-3, No. 2, pp. 105-117, April 1988.

[4] C. T. Rim, D. Y. Hu and G. H. Cho, " The graphical D-Q transformation of general power switching converters," IEEE-IAS Conf. Rec., 1988, pp. 940-945.